Supporting Information

Strain-ultrasensitive surface wrinkles for visual optical sensor

Tianjiao Ma, Shuai Chen, Jin Li, Jie Yin, Xuesong Jiang*

School of Chemistry& Chemical Engineering, Frontiers Science Center for Transformative Molecules, State Key Laboratory for Metal Matrix Composite Materials, Shanghai Jiao Tong University, Shanghai 200240, P. R. China

***Corresponding author.** E-mail: ponygle@sjtu.edu.cn

1. Experimental section

1.1 Materials.

Sodium methanolate and potassium iodide purchased from China National Pharmaceutical Group were used directly without further purification. 9-anthracenemethanol and 4-vinylbenzyl chloride purchased from Adamas-Beta Co. Ltd. were used as received. n-Butyl acrylate obtained from China National Pharmaceutical Group was washed by 5 wt% sodium hydroxide solution and then dried by anhydrous magnesium chloride. Multiwalled carbon nanotubes obtained from J&K Scientific Ltd. were used as received.

1.2 Characterization

^{1}H NMR spectra were recorded on a nuclear magnetic resonance (AVANCE III HD 500) instrument with chloroform-d ($CDCl_3$) as the solvent and tetramethyl silane (TMS) as an internal standard at room temperature. Average molecular weights were determined by means of gel permeation chromatography (GPC, LC-20A, Shimadzu, Japan), using tetrahydrofuran as an eluent at a flow rate of 1.0 mL min^{-1} with a combination of two columns (Shodex, KF-802 and 804, 300 × 8 mm) and equipped with a RID-10A differential refractive index detector. The sample concentration was 2 mg mL^{-1} and the injection volume was 50 μL. Observation of the surface morphology and the measurement of the top-layer film thickness were performed by laser scanning confocal microscopy (LSCM, LEXT OLS5000, Olympus, Japan). The UV light source is LED and the intensity is 15 mW cm^{-2}.

1.3 Synthesis of materials

Synthesis of 9-(4-vinylbenzyloxymethyl) anthracene (VBAN)

9-Anthracenemethanol (6.248 g, 30 mmol), 4-vinylbenzyl chloride (4.579 g, 30 mmol), sodium methanolate (8.103 g, 150 mmol) and potassium iodide (4.98 g, 30 mmol) were dissolved into 100 ml of dried tetrahydrofuran (THF) solvent. Then the reaction system was heated to 50 °C for 24 hours under nitrogen protection. After cooling to room

temperature, the mixture solution was filtered to remove sodium methanolate. The solution was precipitated in cold methanol for three times to obtain yellow solid (VBAN). The yellow solid was collected by filtration and dried in a vacuum oven at 50°C for 12 hours. ^{1}H NMR (500 MHz, $CDCl_3$, δ ppm): 4.73 (s, 2H), 5.29 (d, 1H), 5.52 (s, 2H), 5.81 (d, 1H), 6.77 (q, 1H), 7.39-7.57 (m, 8H), 8.04 (d, 2H), 8.34 (d, 2H), 8.50 (s, 1H).

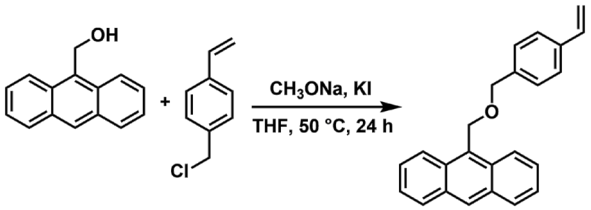

Figure S1. The synthesis of 9-(4-vinylbenzyloxymethyl) anthracene (VBAN).

Synthesis of anthracene-containing polymer (PAN-BA)

The anthracene-containing polymer (PAN-BA) was synthesized by free radical copolymerization. VBAN (5.19 g, 16 mmol) and n-butyl acylate (10.25 g, 80 mmol) were dissolved in 20 mL toluene at a feed molar ration 1:5, and then 154 mg 2,2-azobisisobutyronitrile (AIBN) was added (1 wt% total monomer weight). The polymerization reaction was performed at 70 °C for 24 hours under nitrogen protection. The reaction mixture was precipitated for three times in cold petroleum ether when cooled to room temperature. After the mixture was filtered, the product was dried at 70 °C for 12 hours. At last, we could obtain light yellow solid copolymer (PAN-BA, M_n = 23400, M_w/M_n = 1.75). ^{1}H NMR (500 MHz, $CDCl_3$, δ ppm): 8.59-6.47 (benzene or anthracene ring), 5.61-3.35 (-O-CH_2-), 2.55-0.44 (-CH-CH_2-CH_3).

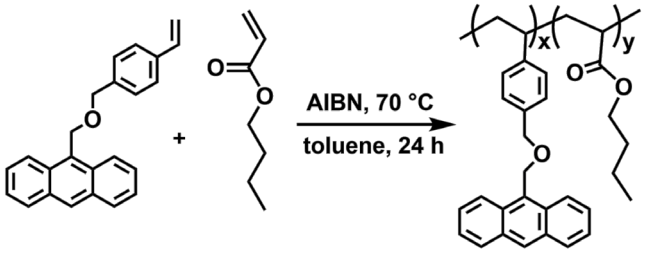

Figure S2. The synthesis of anthracene-containing polymer (PAN-BA).

1.4 Preparation of PDMS substrate

The PDMS elastic sheet was prepared by mixing PDMS prepolymer (Sylgard 184, Dow

Corning) in a 10:1 base/curing agent ratio, followed by drop-coating in a Petri dish, degassing in a vacuum oven, and curing at 70 °C for 4 h (thickness approximately 400 μm). Then the sample was cut into 1 cm × 1 cm squares and 1 cm × 5 cm rectangles.

1.5 Preparation of CNT-PDMS substrate

To reduce the influence of reflection from the background, CNT-containing PDMS was used as the black substrate. PDMS base agent (15 g) and multiwalled carbon nanotubes (15 mg, 0.1 wt%) were mixed in 20 ml toluene and subjected to ultrasonic treatment for 12 h. Then the mixture was dried in an oven at 70 °C for 10 h to remove the solvent. The obtained CNT-containing PDMS base was mixed with 1.5 g curing agent (base/curing agent ratio was 10:1). The mixture was poured into a Petri dish, degassed in a vacuum oven, and cured at 70 °C for 4 h (thickness approximately 400 μm). Then the sample was cut into 1 cm × 1 cm squares and 1 cm × 5 cm rectangles.

1.6 Preparation of surface wrinkle pattern

As for thermal treatment induced wrinkles, a toluene solution of PAN-BA (6 wt%) was spin-coated onto a PDMS sheet to prepare the skin layer. The bilayer samples were irradiated with/without photomask by 365 nm UV light for 15 min and heated at 85 °C. When cooling to room temperature, ordered/random wrinkled patterns occurred. Then the samples were cured on a vernier caliper.

As for prestretching induced wrinkles, a toluene solution of PAN-BA (6 wt%) was spin-coated onto a PDMS sheet to prepare the skin layer. The samples were cured on a vernier caliper and prestretched for 10%. After irradiated by 365 nm UV light for 15 min, 2% or 6% prestrain was released and ordered wrinkled patterns occurred.

1.7 Stretching of surface wrinkle pattern

As for uniaxial stretching, the samples were cured on a vernier caliper and stretched. The applied strain was measured by the vernier caliper. As for equiaxed stretching, the samples underwent thermal treatment. The applied strain was calculated by coefficient of thermal expansion and temperature variation.

2. Results and discussion

2.1 The typical wavelength (λ) and amplitude (A) in the bilayer system

According to linear buckling theory, the classical equation for bending of a stiff film on a more compliant, elastic substrate is

$$\bar{E}_f I \frac{d^4 z}{dx^4} + F \frac{d^2 z}{dx^2} + kz = 0 \tag{S1}$$

Here, $\bar{E}$ and F represent the plane-strain modulus and the uniaxially applied force or load, respectively. The subscript f refers to the skin layer in the bilayer system. I and k refer to the moment of inertia and the Winkler's modulus of an elastic half-space, respectively, which are described by Equations S2 and S3. The z-axis is defined to be normal to the surface and the x-axis parallel to the direction of F. The sinusoidal vertical deflection of the film (z) is described by Equation S4.

$$I = \frac{wh^3}{12} \tag{S2}$$

$$k = \frac{\bar{E}_s w \pi}{\lambda} \tag{S3}$$

$$z(x) = A \sin \frac{2\pi x}{\lambda} \tag{S4}$$

Here, w and h represent the width of the film and its thickness, respectively. The subscript s refers to the substrate in the bilayer system.

Equation S5 is obtained by substituting Equations S3 and S4 into Equation S1.

$$F = 4\bar{E}_f I \left(\frac{\pi}{\lambda}\right)^2 + \frac{\bar{E}_s w}{4} \left(\frac{\pi}{\lambda}\right)^{-1} \tag{S5}$$

Solving Equation S5 yields the typical wavelength and critical force, as given by Equations S6 and S7, respectively.

$$\lambda = 2\pi h \left(\frac{\bar{E}_f}{3\bar{E}_s}\right)^{1/3} \tag{S6}$$

$$F_c = \frac{\bar{E}_f w h}{4} \left(\frac{3\bar{E}_s}{\bar{E}_f}\right)^{2/3} \tag{S7}$$

The critical strain is obtained from Equation S7 and given as Equation S8.

$$\varepsilon_c = \frac{\sigma_c}{\bar{E}_f} = \frac{F_c}{hw\bar{E}_f} = \frac{1}{4}\left(\frac{3\bar{E}_s}{\bar{E}_f}\right)^{2/3} \tag{S8}$$

The amplitude can be calculated from geometric deformation, as shown in Equation S9.

$$\varepsilon - \varepsilon_c = \frac{1}{\lambda}\int_0^{\lambda}\sqrt{1+\left(\frac{dz}{dx}\right)^2}\,dx - 1 \approx \frac{\pi^2 A^2}{\lambda^2} \quad \text{(S9)}$$

Solving Equation S9 yields the typical amplitude, as given by Equation S10.

$$\mathrm{A} = h\sqrt{\frac{\varepsilon-\varepsilon_c}{\varepsilon_c}} \quad \text{(S10)}$$

Here, ε can be described as ε_{pre} - $\varepsilon_{applied}$. Thus, Equation S11 is obtained.

$$A = h\sqrt{\frac{\varepsilon_{pre}-\varepsilon_{applied}-\varepsilon_c}{\varepsilon_c}} \quad \text{(S11)}$$

2.2 The modified amplitude (*A*) in the bilayer system

Owing to the plastic deformation of PDMS, the modified equation for bending of a stiff film on a more compliant, elastic substrate is

$$\bar{E}_f I\frac{d^4z}{dx^4} + F\frac{d^2z}{dx^2} + k(z - z_0) = 0 \quad \text{(S12)}$$

Here, z_0 is the sinusoidal vertical predeflection of the PDMS and described by Equation S13.

$$z_0 = A_0 \sin\frac{2\pi x}{\lambda} \quad \text{(S13)}$$

Here, A_0 represents the amplitude of sinusoidal predeformation of PDMS. λ shows same value with that in Equation S6 due to the preparation process.

By substituting Equations S3, S4 and S13 into Equation S12, Equation S14 is obtained.

$$F = 4\bar{E}_f I\left(\frac{\pi}{\lambda}\right)^2 + \frac{\bar{E}_s w}{4}\left(\frac{\pi}{\lambda}\right)^{-1} - \frac{\bar{E}_s w}{4}\left(\frac{\pi}{\lambda}\right)^{-1}\frac{A_0}{A} \quad \text{(S14)}$$

By substituting Equations S2 and S6 into Equation S14, the modified critical force is obtained and given as Equation S15.

$$F_c' = \frac{\bar{E}_f wh}{4}\left(\frac{3\bar{E}_s}{\bar{E}_f}\right)^{2/3}\left(1 - \frac{2}{3}\frac{A_0}{A}\right) = F_c\left(1 - \frac{2}{3}\frac{A_0}{A}\right) \quad \text{(S15)}$$

The critical strain is obtained from Equation S15 and given as Equation S16.

$$\varepsilon_c' = \frac{\sigma_c'}{\bar{E}_f} = \frac{F_c'}{hw\bar{E}_f} = \varepsilon_c\left(1 - \frac{2}{3}\frac{A_0}{A}\right) \quad \text{(S16)}$$

The amplitude can be calculated from geometric deformation, as shown in Equation S17.

$$\varepsilon - \varepsilon_c' = \frac{1}{\lambda}\int_0^{\lambda}\sqrt{1+\left(\frac{dz}{dx}\right)^2}\,dx - 1 \approx \frac{\pi^2 A^2}{\lambda^2} \quad \text{(S17)}$$

Solving Equation S17 yields the modified amplitude, as given by Equation S18.

$$\mathrm{A} = h\sqrt{\frac{\varepsilon-\varepsilon_c}{\varepsilon_c}+\frac{2}{3}\frac{A_0}{A}} \quad \text{(S18)}$$

Here, ε can be described as ε_{pre} - $\varepsilon_{applied}$. Thus, Equation S19 is obtained.

$$A = h\sqrt{\frac{\varepsilon_{pre}-\varepsilon_{applied}-\varepsilon_c}{\varepsilon_c}+\frac{2}{3}\frac{A_0}{A}} \quad \text{(S19)}$$

2.3 Critical strain to eliminate wrinkles in the bilayer system and two typical modes of external strain

According to linear buckling theory, the critical elimination strain is given by Equation S20.

$$\varepsilon_{critical\ applied} = \varepsilon_{pre} - \varepsilon_c' \quad \text{(S20)}$$

Two typical modes of external strain are shown in Fig. S14. The $\varepsilon_{applied}$ is calculated by Equations S21 and S22 for stretching and bending mode, respectively.

$$\varepsilon_{applied} = \frac{l-l_0}{l_0} = \frac{L-L_0}{L_0} = \varepsilon_{external} \quad \text{(S21)}$$

$$\varepsilon_{applied} = \frac{l-l_0}{l_0} = h_{PDMS}\frac{1}{R} = h_{PDMS}\rho \quad \text{(S22)}$$

Here, l, l_0, h_{PDMS}, L, and L_0 represent the current length of PDMS, the initial length of PDMS, the thickness of PDMS, the current length of foundation, and the initial length of foundation, respectively. $\varepsilon_{external}$ refers to the external strain applying on the foundation in the stretching mode. R and ρ represent the curvature radius and curvature in the bending mode, respectively.

2.4 Average orientation angle ($\bar{\varphi}$) of surface wrinkles

We defined a quantity of average orientation angle ($\bar{\varphi}$) as given in Equation S23 to describe the average orientation of wrinkles.

$$\bar{\varphi} = \frac{\sum \varphi \cdot l \cdot A}{\sum l \cdot A} \quad \text{(S23)}$$

Here, in a small element of wrinkle, φ represent the included angle between strain direction and wave crest, which is perpendicular to the wrinkle direction (θ_W). l, and A represent the length of wave crest, and amplitude, respectively. Thus, $\bar{\varphi}$ represents the weighted average included angle between wave crest and strain direction for a group of wrinkles.

2.5 Viewable angle (δ) of the reflected optical signals

As shown in Fig. S17, z-axis is defined to be normal to the surface and x-axis parallel to the direction of wrinkle. The blue, grey, red and green planes were xz-plane, tangent plane of the wrinkle profile, orthogonal plane of surface, and orthogonal plane of grey plane, respectively. The red solid line and dotted line represent the light and the image of reflected light, respectively. α and β refer to the included angle between incident light and z-axis, and included angle between projection of incident light on the surface and x-axis, respectively.

According to geometry, the included angle between incident angle and its projection on xz-plane (α') and the included angle between projection of incident light on the xz-plane and z-axis (α'') were described in Equations S24 and S25, respectively.

$$\sin\alpha' = \sin\alpha \sin\beta \tag{S24}$$

$$\tan\alpha'' = \tan\alpha \cos\beta \tag{S25}$$

γ is the inclination angle of wrinkle profile, which is described in Equations S26 and S27.

$$\tan\gamma\,(x) = A\frac{2\pi}{\lambda}\cos\frac{2\pi x}{\lambda} \tag{S26}$$

$$\gamma_{max} = \tan^{-1} A\frac{2\pi}{\lambda} \tag{S27}$$

According to geometry, the include angle between incident light and the image of reflected light ($\angle AOA'$) can be calculated by Equation S28.

$$\angle AOA' = 2\angle AOO' = 2\sin^{-1}[\cos\alpha' \sin(\gamma + \alpha'')] \tag{S28}$$

Thus,

$$\angle AOA' = 2\sin^{-1}\left[\frac{\sqrt{1-\sin^2\alpha\sin^2\beta}}{\sqrt{1+\tan^2\alpha\cos^2\beta}}(\sin\gamma + \cos\gamma\tan\alpha\cos\beta)\right] \tag{S29}$$

2δ is defined as the maximum included angle of reflected lights, which is equal to the maximum included angle of all possible OA's. Thus,

$$2\delta = \sin^{-1}\left[\frac{\sqrt{1-\sin^2\alpha\sin^2\beta}}{\sqrt{1+\tan^2\alpha\cos^2\beta}}(\sin\gamma_{max} + \cos\gamma_{max}\tan\alpha\cos\beta)\right] + \sin^{-1}\left[\frac{\sqrt{1-\sin^2\alpha\sin^2\beta}}{\sqrt{1+\tan^2\alpha\cos^2\beta}}(\sin\gamma_{max} - \cos\gamma_{max}\tan\alpha\cos\beta)\right] \tag{S30}$$

For some special cases, if $\beta = 0$,

$$2\delta = \gamma_{max} \tag{S31}$$

If $\beta = 90°$,

$$2\delta = \sin^{-1}(\cos\alpha \sin\gamma_{max}) \tag{S32}$$

The Viewable angle (δ) can also be obtained experimentally. According to geometry, δ is calculated by utilizing the reflected light diffraction pattern. The result is given in Equation S33.

$$\delta = \tan^{-1}\frac{r}{d} \tag{S33}$$

Here, r represents the radius of the diffraction pattern, and d refers to the distance between the sample and the screen.

3. Supplementary figures

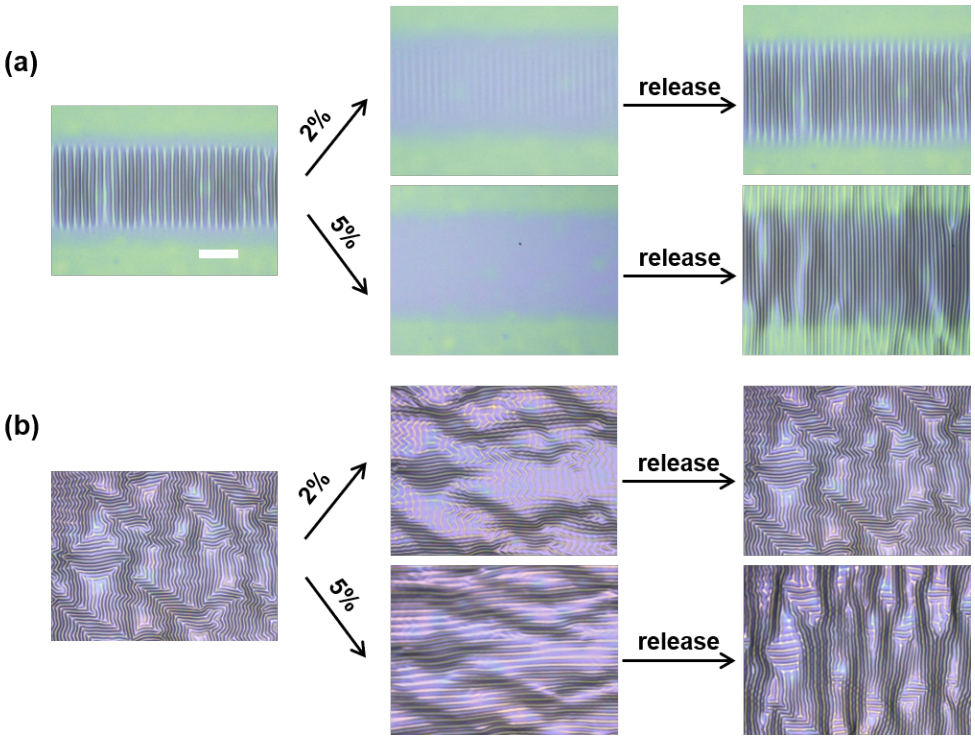

Figure S3. The topography evolution and reversible stretching range of (a) ordered wrinkles and (b) random wrinkles under applied strain in parallel direction. Scale bar: 100 μm.

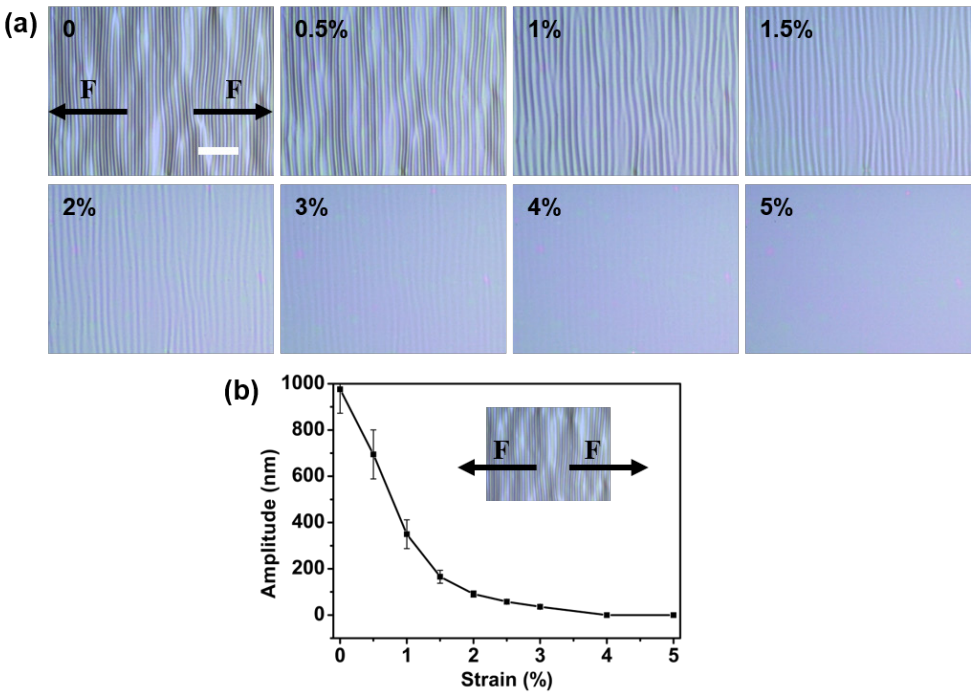

Figure S4. (a) Laser scanning confocal microscope (LSCM) images of prestretching induced wrinkles under applied strain in parallel direction. Scale bar: 100 μm. (b) Amplitude (A) of prestretching induced ordered wrinkles as a function of applied strain in parallel direction.

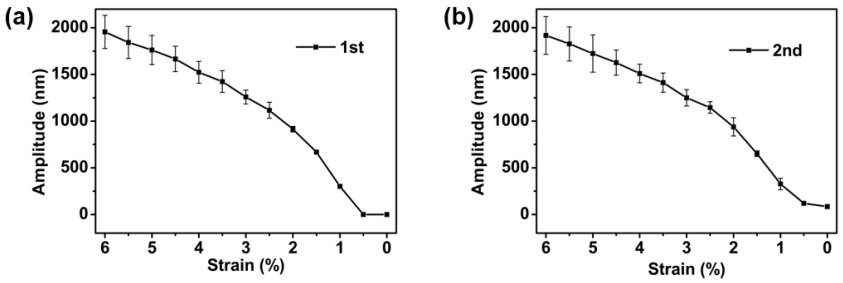

Figure S5. Amplitude (*A*) of prestretching induced wrinkles as a function of prestrain during (a) the first compressive processing and (b) the second compressive processing.

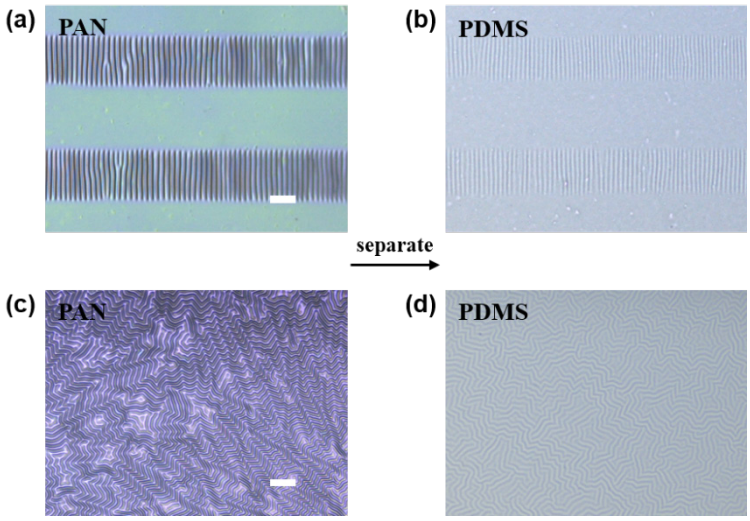

Figure S6. Topography of PDMS after separating the top film. (a) Ordered wrinkles in the bilayer system. (b) Topography of PDMS beneath ordered wrinkled film. (c) Random wrinkles in the bilayer system. (d) Topography of PDMS beneath random wrinkled film. Scale bar: 100 μm.

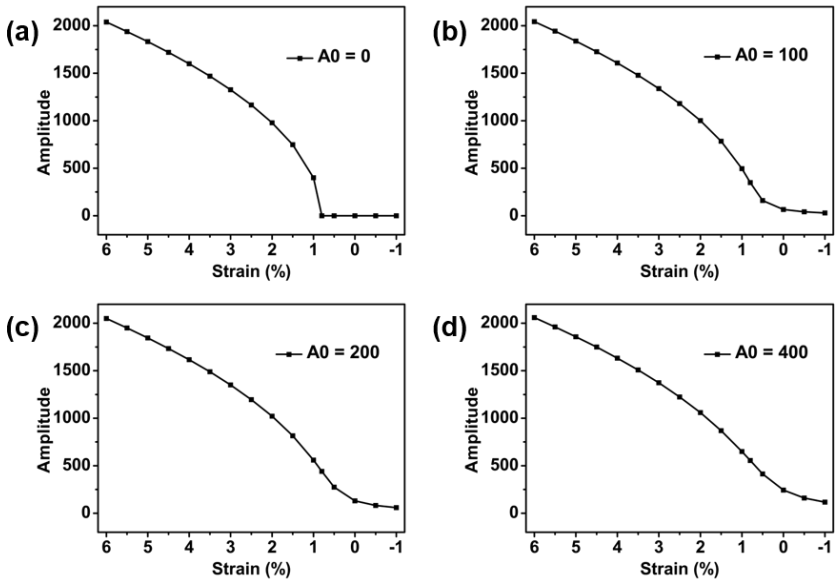

Figure S7. Amplitude (A) as a function of strain with different amplitudes (A_0) of sinusoidal predeformation of substrate. (a) A_0= 0. (b) A_0= 100. (c) A_0= 200. (d) A_0= 400.

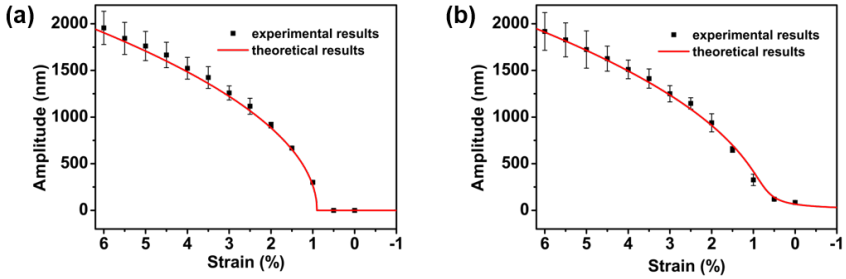

Figure S8. Amplitude (A) of prestretching induced wrinkles as a function of strain during (a) the first compressive processing and (b) the second compressive processing.

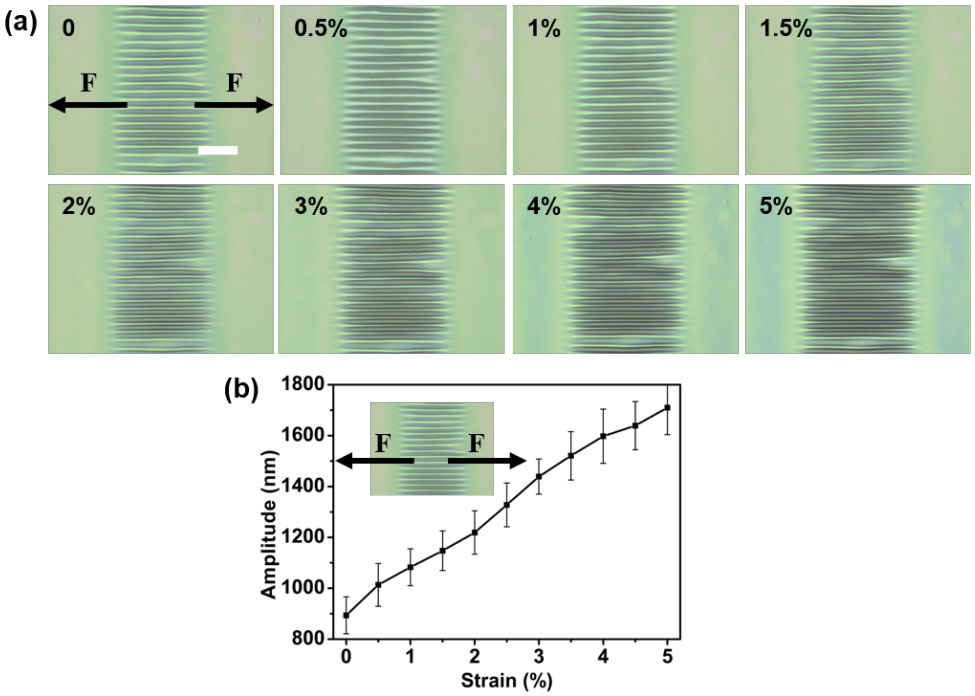

Figure S9. (a) LSCM images of ordered wrinkles under applied strain in perpendicular direction. Scale bar: 100 μm. (b) Amplitude (*A*) of ordered wrinkles as a function of applied strain in perpendicular direction.

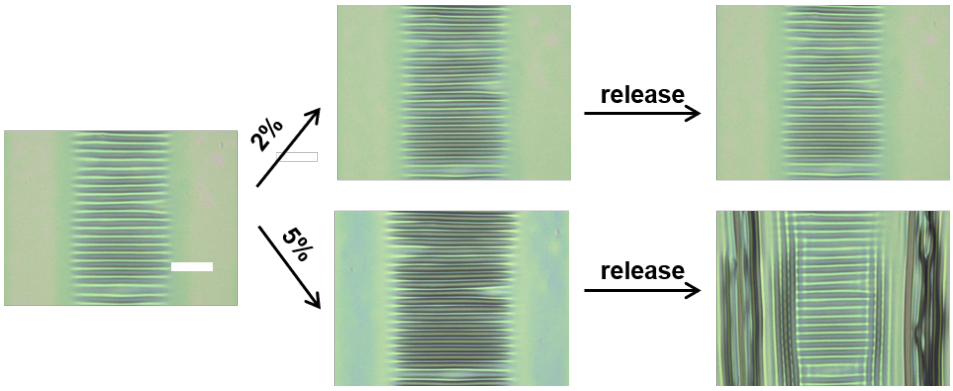

Figure S10. The topography evolution and reversible stretching range of ordered wrinkles under applied strain in perpendicular direction. Scale bar: 100 μm.

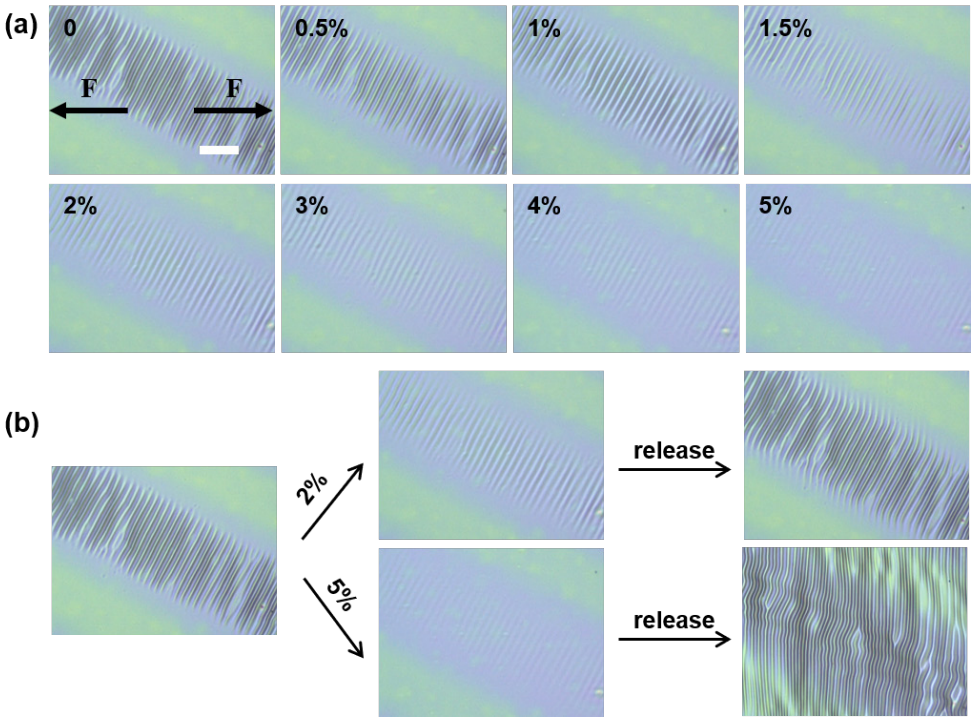

Figure S11. (a) LSCM images of ordered wrinkles under applied strain in 30° direction. (b) The topography evolution and reversible stretching range of ordered wrinkles under applied strain in 30° direction. Scale bar: 100 μm.

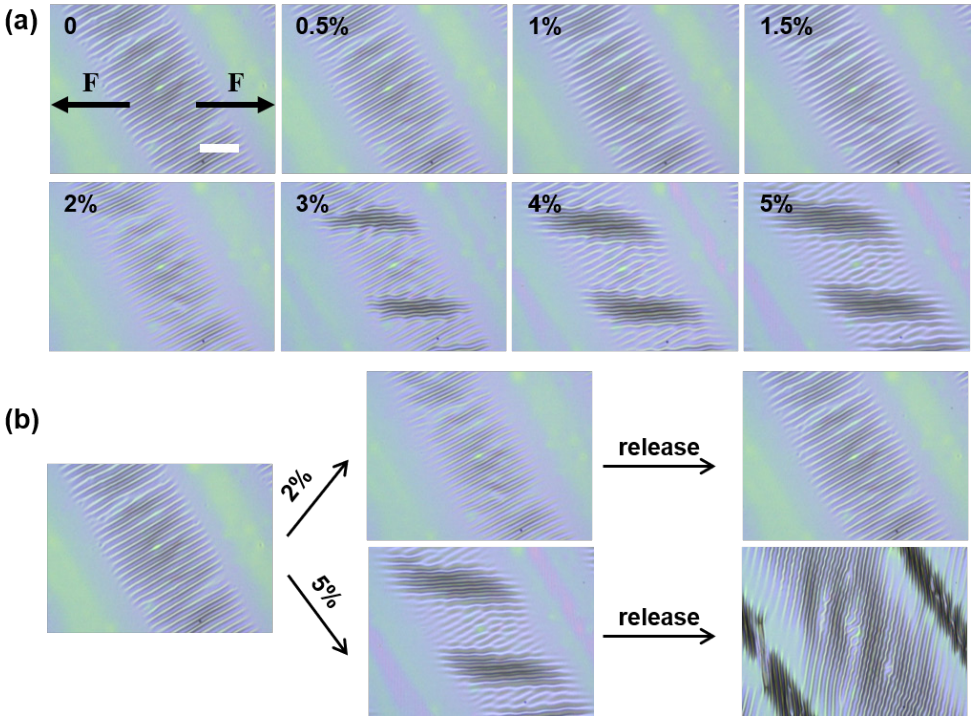

Figure S12. (a) LSCM images of ordered wrinkles under applied strain in 60° direction. (b) The topography evolution and reversible stretching range of ordered wrinkles under applied strain in 60° direction. Scale bar: 100 μm.

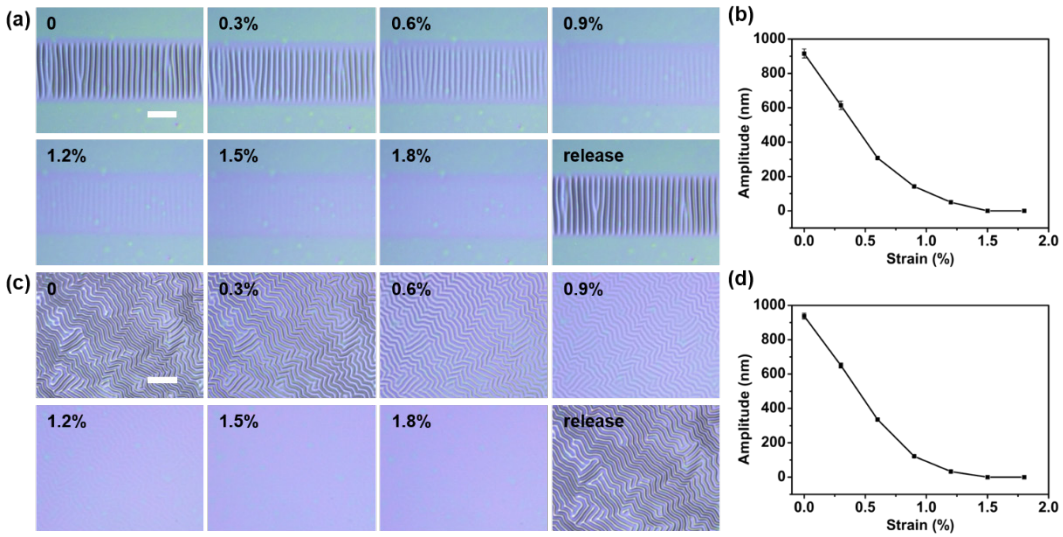

Figure S13. (a) LSCM images of ordered wrinkles under equiaxed strain. (b) Amplitude (*A*) of ordered wrinkles as a function of equiaxed strain. (c) LSCM images of random wrinkles under equiaxed strain. (d) Amplitude (*A*) of random wrinkles as a function of equiaxed strain. Scale bar: 100 μm.

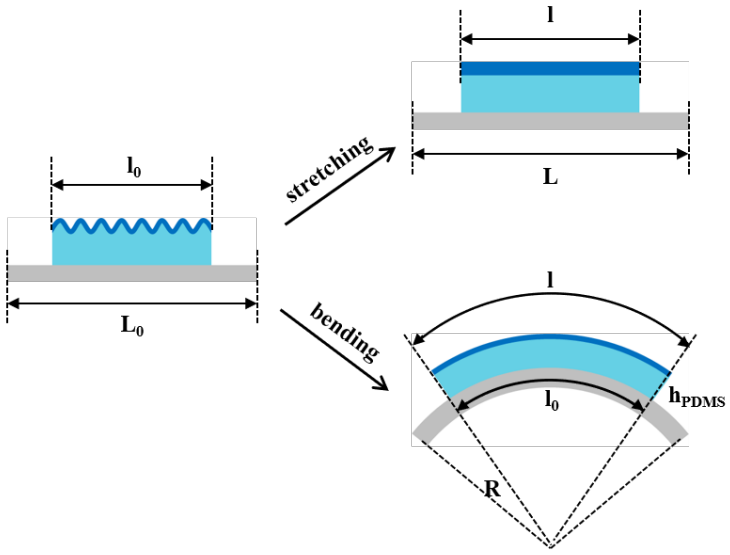

Figure S14. Schematic illustration of two typical modes of surface wrinkles ultrasensitive to external strain: Stretching and Bending.

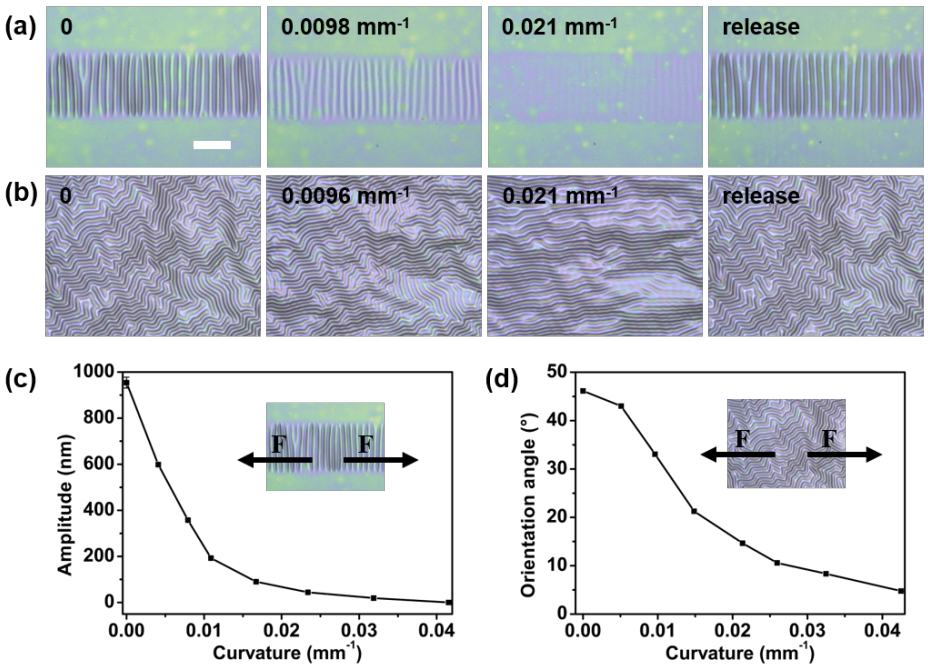

Figure S15. Topography evolution of wrinkles during bending. (a) LSCM images of ordered wrinkles during bending in parallel direction. (b) LSCM images of random wrinkles during bending. Scale bar: 100 μm. (c) Amplitude (A) of ordered wrinkles as a function of curvature in parallel direction. (d) Average orientation angle ($\bar{\varphi}$) of random wrinkles as a function of curvature.

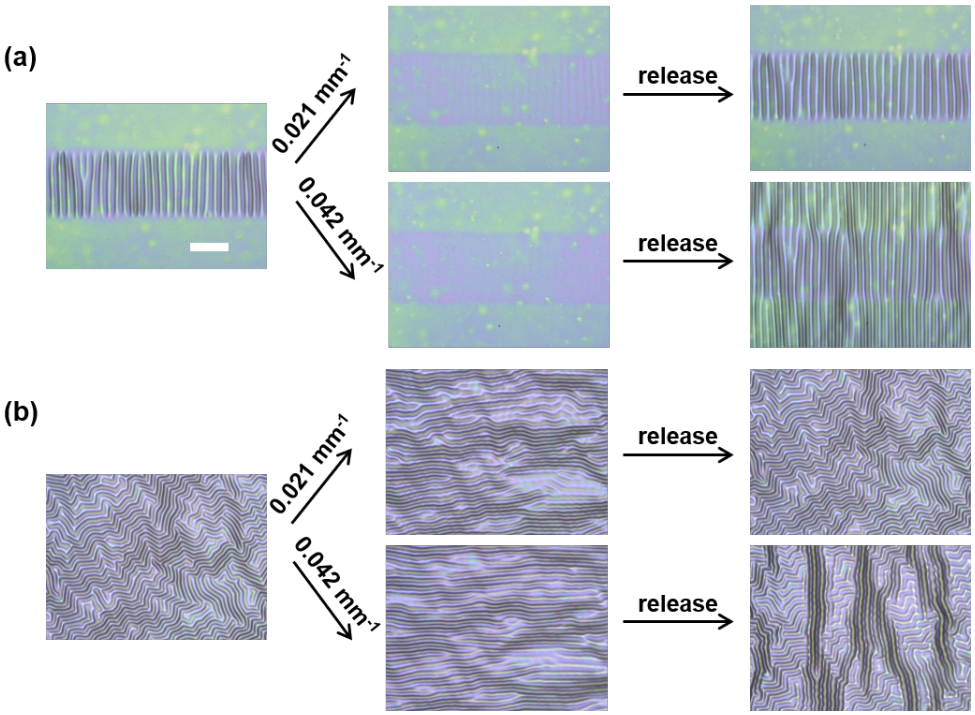

Figure S16. The topography evolution and reversible bending range of (a) ordered wrinkles and (b) random wrinkles during bending in parallel direction. Scale bar: 100 μm.

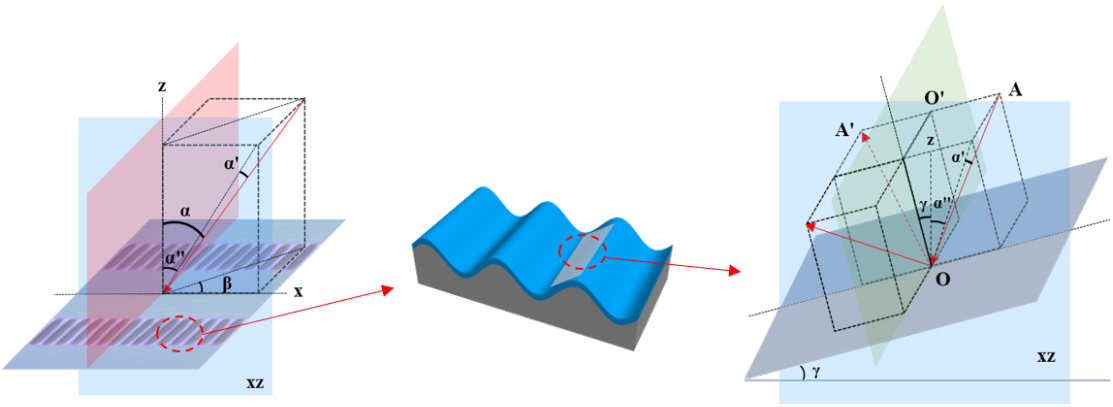

Figure S17. Schematic illustration of reflected light by surface wrinkles.

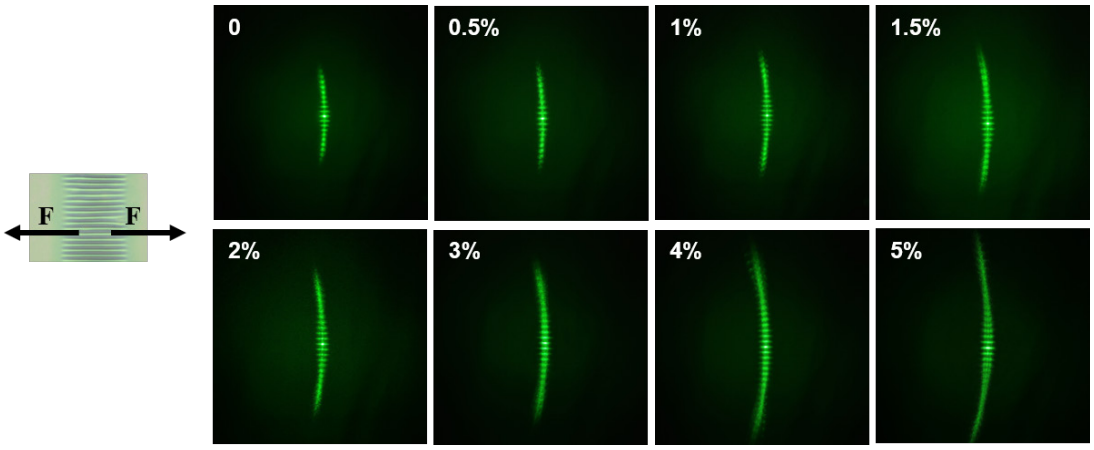

Figure S18. Images of reflected diffraction pattern evolution corresponding with ordered wrinkles under strain in perpendicular direction.

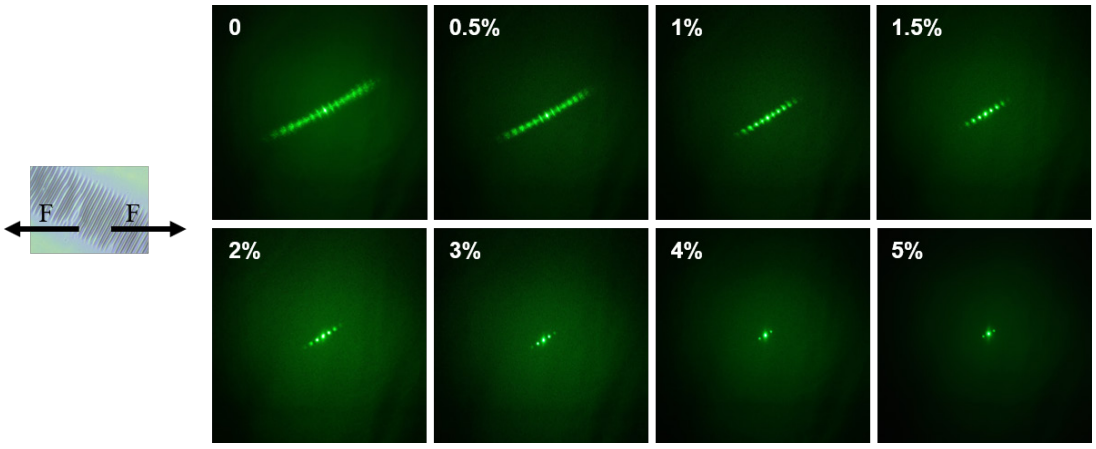

Figure S19. Images of reflected diffraction pattern evolution corresponding with ordered wrinkles under strain in 30° direction.

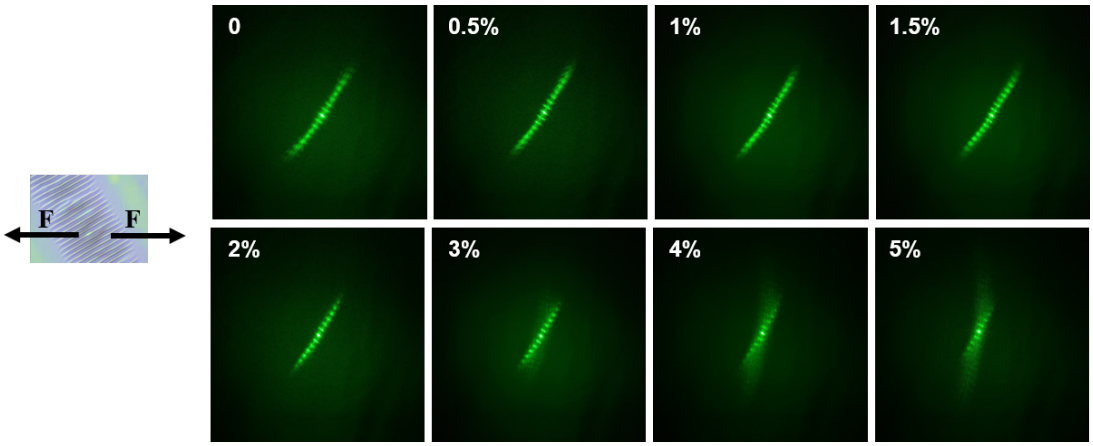

Figure S20. Images of reflected diffraction pattern evolution corresponding with ordered wrinkles under strain in 60° direction.

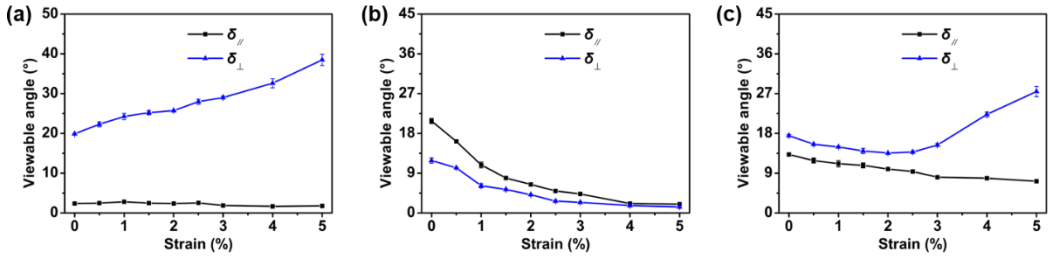

Figure S21. Ordered wrinkles corresponding viewable angles as a function of strain in the (a) perpendicular (b) 30° (c) 60° direction.

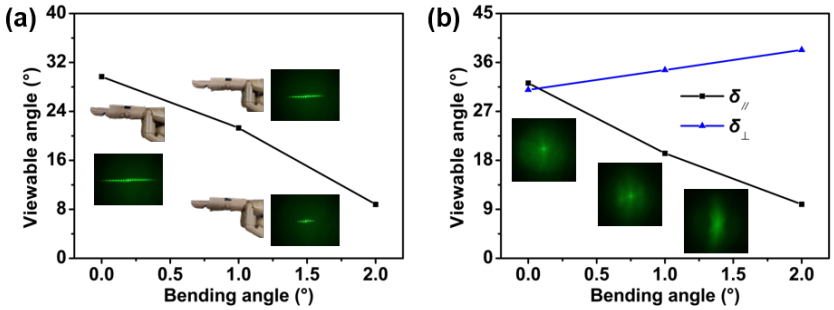

Figure S22. Viewable angle and reflected diffraction pattern evolution corresponding with (a) ordered wrinkles and (b) random wrinkles during a prosthetic finger bending.

4. Supplementary movies

Movie S1. In-situ observation of color change of an ordered wrinkles-based sensor attached to the joint during slightly bending of the human wrist.

Movie S2. In-situ observation of reflected diffraction pattern evolution corresponding with ordered wrinkles and random wrinkles attached to the joint during slightly bending of the human wrist.

Movie S3. In-situ observation of color change of an ordered wrinkles-based sensor attached to the joint during slightly bending of the human finger.